Theoretical Study of Quantum Spin Liquid Candidate $Na_2BaCo(PO_4)_2$

Rebecca Chan

Center for Emergent Materials, The Ohio State University

July 2021

Abstract

Recent experimental evidence demonstrates that $Na_2BaCo(PO_4)_2$ is a candidate material to realize the quantum spin liquid (QSL). This compound can be described by the Ising-Kitaev-Gamma model on a triangular lattice. Using Python's QuSpin package and the exact diagonalization method, we simulate this model in a 4×4 cluster with periodic boundary conditions, obtaining a quantum phase diagram for this system. We analyze the ordering patterns of the observed phases by calculating spin structure factors. Focusing on the $\Gamma = 0$ case, there is a ferromagnetic regime for large, negative J_z/K as expected classically. There is also a 2×2 in-plane ordered phase for around $-0.3 < J_z/K < 1.2$. Most importantly, for $J_z/K > 1.2$, there is a phase that lacks magnetic order and which may be a quantum spin liquid phase.

1 Background

Quantum spin liquids (QSLs) are distinct quantum states of matter that feature long range entanglement and the absence of order in the ground state[1]. They cannot be expressed as a product state, but rather an entangled superposition of many product states, where the measurement of one observable influences the result of the measurements of others. Unlike classical magnetic orders, strong quantum fluctuations prevent spins from ordering so they remain in a disordered liquid-like state even near zero temperature. Their highly entangled nature enables them to have many unique physical properties, including the ability to support anyons, exotic excitations that do not obey fermionic or bosonic statistics. Non-Abelian anyons can potentially serve as qubits for topological quantum computation, making QSLs a compelling topic to study.

One of the main challenges is to find a material that has a QSL phase. Recent experimental evidence by Zhong et al. indicates that $Na_2BaCo(PO_4)_2$—a compound that consists of $Co_2{}^+$ with effective S=1/2 on a geometrically frustrated triangular lattice—is a QSL candidate. Magnetic susceptibility and neutron scattering experiments observe no long-range magnetic ordering or glassy behavior down to 0.05 K in this compound, and thermodynamic measurements demonstrate an immense amount of magnetic entropy present below 1 K in the absence of a magnetic field[2].

Our goal is to study this material theoretically by numerically modeling its ground state. Gdanski and Lu (unpublished) have fitted theoretical linear spin wave dispersion data to inelastic neutron scattering data to determine a model for $Na_2BaCo(PO_4)_2$ (Fig. 1). Note that a magnetic field needs to be applied in order to polarize the spins, stabilize an ordered ground state, and generate a spin wave. One can then use linear spin wave theory to determine the parameters of the theoretical spin model for the material. Gdanski and Lu found that the minimal model up to nearest neighbor (NN) interactions is the Ising-Kitaev-Gamma model on a triangular lattice. We will use a 4×4 finite lattice with periodic boundary conditions (PBC) to understand the phases and phase diagram of the model, in the absence of a magnetic field.

This model cannot be solved analytically, so we turn to a numerical approach. Our search for highly entangled phases of matter means that numerical studies should identify ground states that cannot be continuously deformed into a product state while remaining in the same phase[1]. Broadly, "continuous deformation" corresponds to continuous changes of a ground state wavefunction due to varying the parameter(s) of the Hamiltonian. Therefore, we should first use numerical methods to look for plausible QSL phases in the quantum phase diagrams. Then there are two things that we want to detect numerically for each phase. The

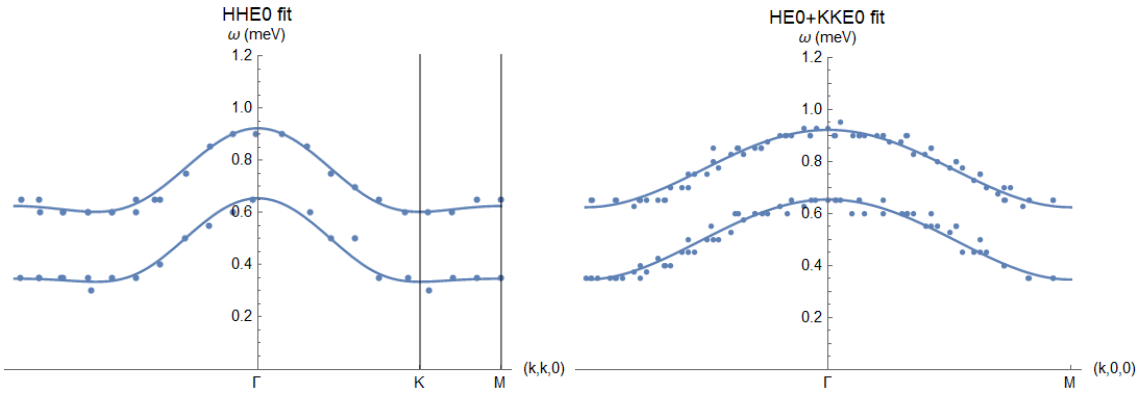

Figure 1: Comparison of theoretical linear spin wave dispersion (solid lines) and inelastic neutron scattering data (discrete points). The applied magnetic field is $B_z = 3\ T$ (lower curve) and $B_z = 4\ T$ (upper curve) for the two curves in each figure.

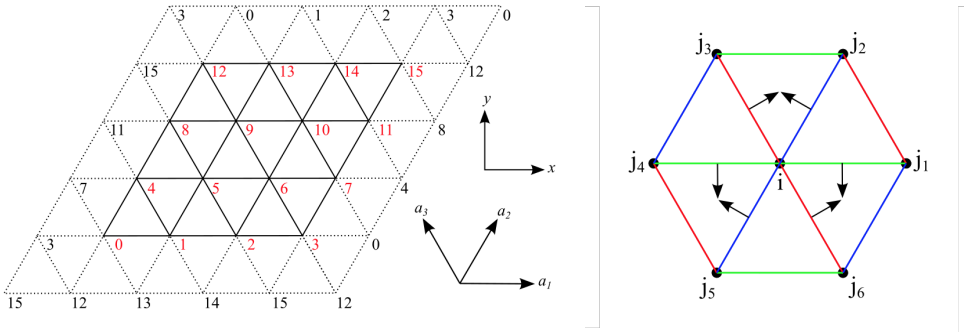

(a) (b)

Figure 2: The triangular lattice setup. The black arrows in (b) indicate the β_{ij} direction for each NN link. Each site has six nearest neighbors but only three need to be considered per central site i—one link of each color—because each $\langle i, j\rangle$ pair should only be counted once. Here we will use j_1, j_2, and j_3.

first is the absence of order—we want to see order parameters vanish so that they do not break symmetry. The absence of order can be measured by calculating the spin structure factor for parameters within the phase. The second is long range entanglement in the ground state, which can be detected by verifying that the topological entanglement entropy is non-zero[1]. If these two checks pass, then we have likely found a QSL phase.

2 Methods

To understand the triangular lattice setup, consider a generic spin-$\frac{1}{2}$ model on a triangular lattice with $n_x \times n_y$ PBC. For simplicity, define unit vectors

$$\mathbf{a}_1 = \hat{x}, \quad \mathbf{a}_2 = \tfrac{1}{2}\hat{x} + \tfrac{\sqrt{3}}{2}\hat{y}, \quad \mathbf{a}_3 = -\tfrac{1}{2}\hat{x} + \tfrac{\sqrt{3}}{2}\hat{y}. \tag{1}$$

as shown in Fig. 2a. We can label each of the $N = n_x \times n_y$ sites by its position in the $x - y$ plane, $\mathbf{r} = x_1\mathbf{a}_1 + x_2\mathbf{a}_2$, $x_i \in \mathbb{Z}$. Let $\hat{r}_{ij} = (\mathbf{r}_i - \mathbf{r}_j)/|\mathbf{r}_i - \mathbf{r}_j|$ indicate the direction of the link between NN sites i and j. We can also label each site by an integer $i \in \{0, \ldots, N-1\}$ where $i = x_1 + x_2 n_y$. Note that PBC imply that a site at $x_1\mathbf{a}_1 + x_2\mathbf{a}_2$ has the same label as the site at $(x_1 + cn_x)\mathbf{a}_1 + (x_2 + dn_y)\mathbf{a}_2$ for any $c, d \in \mathbb{Z}$. In addition, using modular arithmetic, if site i located at $x_1\mathbf{a}_1 + x_2\mathbf{a}_2$ for $x_1, x_2 \in \mathbb{Z}$ then the three NN sites

are located as follows:

$$\begin{aligned} j_1 &\to (x_1+1) \mod n_x\,\mathbf{a}_1 + x_2\,\mathbf{a}_2 \\ j_2 &\to x_1\,\mathbf{a}_1 + (x_2+1) \mod n_y\,\mathbf{a}_2 \\ j_3 &\to (x_1-1) \mod n_x\,\mathbf{a}_1 + (x_2+1) \mod n_y\,\mathbf{a}_2 \end{aligned} \tag{2}$$

The Ising-Kitaev-Gamma Hamiltonian is

$$H = \sum_{\langle i,j\rangle} J_z S_i^z S_j^z + K(\mathbf{S}_i\cdot\hat{r}_{ij})(\mathbf{S}_j\cdot\hat{r}_{ij}) + \Gamma(S_i^{\beta_{ij}} S_j^z + S_i^z S_j^{\beta_{ij}}) \tag{3}$$

where $\langle i,j\rangle$ indicates that i and j are NN pairs. Each pair is only counted once. J_z, K, and Γ are the Ising, Kitaev, and Gamma coupling constants, respectively. We have estimates for J_z and K from the linear spin wave fit, namely $J_z \approx 0.12$ MeV and $K \approx 0.14$ MeV. However, the linear spin wave fit is unable to determine Γ so a numerical approach will be useful. S_i^μ is the μ component of the $S=\frac{1}{2}$ spin operator at site i. The Ising term focuses on the spin component pointing perpendicular to the two-dimensional plane. It is independent of the bond directions, unlike the Kitaev and Gamma terms. The Kitaev term describes interactions that have spin components parallel to the bond direction. $S_i^{\beta_{ij}}$ in the Gamma term is the spin component that is perpendicular to $\hat{r}_{ij}$ in the xy plane. More specifically, $S_i^{\beta_{ij}} = -S_i^y,\ \frac{1}{2}(-\sqrt{3}S_i^x + S_i^y),\ -\frac{1}{2}(S_i^x + \sqrt{3}S_i^y)$ for NN links along the $\pm\mathbf{a}_1,\ \pm\mathbf{a}_2,\ \pm\mathbf{a}_3$ directions, respectively.

The i^{th} Kitaev term is

$$\begin{aligned} K\sum_{j\in\{j_1,j_2,j_3\}} (\mathbf{S}_i\cdot\hat{r}_{ij})(\mathbf{S}_j\cdot\hat{r}_{ij}) &= K\left[(S_i\cdot\hat{r}_{ij_1})(S_{j_1}\cdot\hat{r}_{ij_1}) + (S_i\cdot\hat{r}_{ij_2})(S_{j_2}\cdot\hat{r}_{ij_2}) + (S_i\cdot\hat{r}_{ij_3})(S_{j_3}\cdot\hat{r}_{ij_3})\right] \\ &= K\left[(S_i\cdot\mathbf{a}_1)(S_{j_1}\cdot\mathbf{a}_1) + (S_i\cdot\mathbf{a}_2)(S_{j_2}\cdot\mathbf{a}_2) + (S_i\cdot\mathbf{a}_3)(S_{j_3}\cdot\mathbf{a}_3)\right] \\ &= K\left[S_i^{\mathbf{a}_1}S_{j_1}^{\mathbf{a}_1} + S_i^{\mathbf{a}_2}S_{j_2}^{\mathbf{a}_2} + S_i^{\mathbf{a}_3}S_{j_3}^{\mathbf{a}_3}\right] \end{aligned} \tag{4}$$

In terms of S^x and S^y,

$$\begin{aligned} K\sum_{j\in\{j_1,j_2,j_3\}} (\mathbf{S}_i\cdot\hat{r}_{ij})(\mathbf{S}_j\cdot\hat{r}_{ij}) &= K\left[S_i^xS_{j_1}^x + \left(\tfrac{1}{2}S_i^x + \tfrac{\sqrt{3}}{2}S_i^y\right)\left(\tfrac{1}{2}S_{j_2}^x + \tfrac{\sqrt{3}}{2}S_{j_2}^y\right) + \left(-\tfrac{1}{2}S_i^x + \tfrac{\sqrt{3}}{2}S_i^y\right)\left(-\tfrac{1}{2}S_{j_3}^x + \tfrac{\sqrt{3}}{2}S_{j_3}^y\right)\right] \\ &= K\left[S_i^xS_{j_1}^x + \tfrac{1}{4}\left(S_i^xS_{j_2}^x + S_i^xS_{j_3}^x\right) + \tfrac{3}{4}\left(S_i^yS_{j_2}^y + S_i^yS_{j_3}^y\right)\right. \\ &\qquad \left. + \tfrac{\sqrt{3}}{4}\left(S_i^xS_{j_2}^y + S_i^yS_{j_2}^x - S_i^xS_{j_3}^y - S_i^yS_{j_3}^x\right)\right] \end{aligned} \tag{5}$$

The i^{th} Gamma term is

$$\begin{aligned} \Gamma\sum_{j\in\{j_1,j_2,j_3\}} (S_i^{\beta_{ij}}S_j^z + S_i^zS_j^{\beta_{ij}}) = \Gamma\Big[&-S_i^yS_{j_1}^z - S_i^zS_{j_1}^y + \tfrac{1}{2}(-\sqrt{3}S_i^x + S_i^y)S_{j_2}^z + \tfrac{1}{2}S_i^z(-\sqrt{3}S_{j_2}^x + S_{j_2}^y) \\ &+ \tfrac{1}{2}(\sqrt{3}S_i^x + S_i^y)S_{j_3}^z + \tfrac{1}{2}S_i^z(\sqrt{3}S_{j_3}^x + S_{j_3}^y)\Big] \end{aligned} \tag{6}$$

Using Python's QuSpin package and exact diagonalization, we solved for the energies of the Ising-Kitaev-Gamma model for various parameter values, fixing $K=1$. We also checked the accuracy of the 4×4 PCB triangular lattice part of our code by benchmarking it with the spin-$\frac{1}{2}$ Heisenberg model. NumPy's gradient method helped us calculate the first and second derivatives of the energy with respect to J_z or Γ.

The spin structure factor for $\alpha-\beta$ correlations ($\alpha,\beta = x,y,z$) is defined as

$$F^{\alpha\beta}(\mathbf{q},t) = \left\langle S_{\mathbf{q}}^\alpha(t)\, S_{-\mathbf{q}}^\beta(0)\right\rangle \tag{7}$$

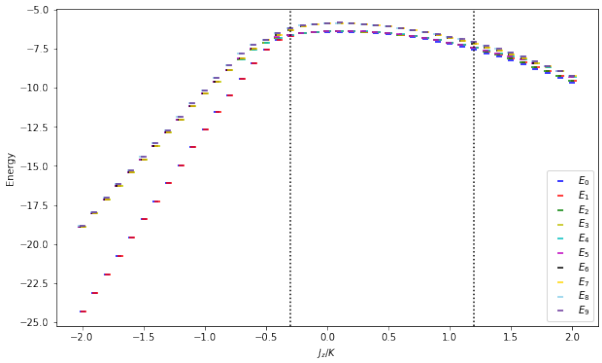

Figure 3: The first ten energy eigenvalues for $\Gamma = 0$ and different J_z. The vertical dotted lines delineate where the behavior of the spectrum changes.

where $\mathbf{q}$ is momentum and t is time. Furthermore,

$$\begin{aligned} S^{\alpha}_{\mathbf{q}}(t) &= \frac{1}{\sqrt{N}} \sum_{\mathbf{r}} e^{-i\mathbf{q}\cdot\mathbf{r}} S^{\alpha}_{\mathbf{r}}(t) \\ &= \frac{1}{\sqrt{N}} \sum_{\mathbf{r}} e^{-i\mathbf{q}\cdot\mathbf{r}} U^{\dagger}(t) S^{\alpha}_{\mathbf{r}}(0) U(t) \\ &= \frac{1}{\sqrt{N}} \sum_{\mathbf{r}} e^{-i\mathbf{q}\cdot\mathbf{r}} e^{iHt} S^{\alpha}_{\mathbf{r}}(0) e^{-iHt} \end{aligned} \tag{8}$$

where $\mathbf{r}$ is the real space position of each lattice site. Plugging in,

$$\begin{aligned} F^{\alpha\beta}(\mathbf{q}, t) &= \frac{1}{N} \left\langle \sum_{\mathbf{r}_j} e^{-i\mathbf{q}\cdot\mathbf{r}_j} e^{iHt} S^{\alpha}_{\mathbf{r}_j}(0) e^{-iHt} \sum_{\mathbf{r}_k} e^{i\mathbf{q}\cdot\mathbf{r}_k} S^{\beta}_{\mathbf{r}_k}(0) \right\rangle \\ &= \frac{1}{N} \left\langle \sum_{\mathbf{r}_j} \sum_{\mathbf{r}_k} e^{-i\mathbf{q}\cdot(\mathbf{r}_j - \mathbf{r}_k)} e^{iHt} S^{\alpha}_{\mathbf{r}_j}(0) e^{-iHt} S^{\beta}_{\mathbf{r}_k}(0) \right\rangle \\ &= \frac{1}{N} \langle \psi_0 | \left[\sum_{\mathbf{r}_j} \sum_{\mathbf{r}_k} e^{-i\mathbf{q}\cdot(\mathbf{r}_j - \mathbf{r}_k)} e^{iHt} S^{\alpha}_{\mathbf{r}_j}(0) e^{-iHt} S^{\beta}_{\mathbf{r}_k}(0) \right] | \psi_0 \rangle \end{aligned} \tag{9}$$

where $|\psi_0\rangle$ is the ground state ket. When $t = 0$, the static spin structure factor indicates the ordering pattern of the ground state. For example, if $\alpha = \beta = z$ and J_z is large and negative, there is a large, sharp peak at $\mathbf{q} = 0$ because those parameters indicate a ferromagnetic ground state. When $t \neq 0$ the dynamical spin structure factor provides information regarding the excitation spectrum of the system.

The total spin structure factor is defined as

$$F(\mathbf{q}, t) = \langle \mathbf{S}_{\mathbf{q}}(t) \cdot \mathbf{S}_{-\mathbf{q}}(0) \rangle = F^{xx}(\mathbf{q}, t) + F^{yy}(\mathbf{q}, t) + F^{zz}(\mathbf{q}, t). \tag{10}$$

It indicates the spin correlations in the x, y, and z directions, providing a better overview of the ordering pattern than $F^{\alpha\beta}$ individually.

3 Results

3.1 Energy Spectrum

Fig. 3 splits the energy spectrum for $\Gamma = 0$ into three main categories. For $J_z < -0.3$, there is two-fold degeneracy ($E_0 = E_1$). Higher energy eigenstates group together but are significantly larger than the ground

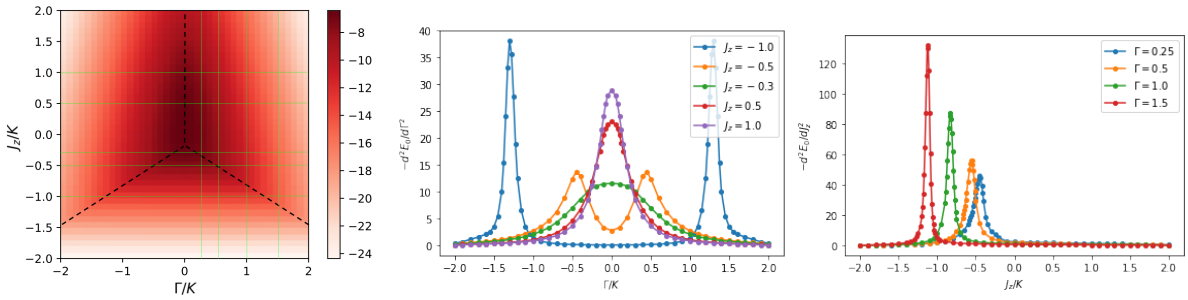

(a) (b) (c)

Figure 4: (a) Ground state energies for different J_z and Γ. The sign of Γ does not affect the energy because a spin rotation along the z axis by 180° will only negate Γ and not J_z or K. The green lines correspond to the derivative plots in (b) and (c). The derivative plots indicate that the phase boundaries are along the three black dashed lines in (a)

state. For $-0.3 < J_z < 1.2$, the ground state energy is very close to the first few excited states. There is a significant gap between these energies and those of the next few excited states. For $J_z > 1.2$, the ground state energy is nondegenerate but relatively close to the those of the excited states. The energy spectrum suggests that we can characterize the system's behavior into three groups, at least for $\Gamma = 0$.

3.2 Quantum Phase Diagram

A singularity in the derivative (of any order) of E_0 with respect to one of the system parameters indicates a phase transition. We can visualize a phase diagram for the model by plotting the second derivative of E_0 with respect to J_z for fixed Γ, as well as with respect to Γ for fixed J_z. For example, Fig. 4c indicates that there is a phase boundary near $J_z = -1.2$ and $\Gamma = 1.5$ if $K = 1$, since that is where there is a sharp peak in the second derivative plot. By locating singularities, we found that the phase boundaries match the features of the ground state energy, as shown in Fig. 4a. Fig. 4b also demonstrates that there is a critical point close to $J_z^* \approx -0.4$ because $-d^2E_0/d\Gamma^2$ morphs from having two peaks for $J_z < J_z^*$ to only one, centered at $\Gamma/K = 0$, for $J_z > J_z^*$.

3.3 Static Spin Structure Factor, $\Gamma = 0$

We expect a ferromagnetic phase when J_z/K is large and negative and $K > 0$. The Ising term dominates, and these values are known to engender ferromagnetic behavior. Fig. 5d supports this ordering pattern since there is a large, sharp peak that comes predominantly from zz correlations—the value of the peak of the zz plot is more than ten times greater than the maximum of the xx or yy plots. The system transitions from this ferromagnetic phase to an ordered phase as J_z increases. For $\Gamma = 0$, this transition occurs near $J_z \approx -0.3$.

Fig. 5h indicates a 2×2 in-plane ordered phase. It is "in-plane" because the xx and yy correlations are dominant. The peaks are located on the centers of the edges of the Brillouin zone. The phase is "2×2" because the unit cell is doubled.

Lastly, Fig. 5l demonstrates the absence of order for larger J_z. The xx, yy, and zz components are all around the same magnitude, indicating that the spins do not particularly prefer one direction over the other. Static spin structure factor plots for plausible QSL phases should lack sharp peaks and be more uniform, making this third phase promising.

4 Conclusion

We have studied a model for the QSL candidate $Na_2BaCo(PO_4)_2$. A summary of our main results for $\Gamma = 0$ is in Table 1. Most importantly, our numerical results suggest that there may be a QSL phase for small Γ

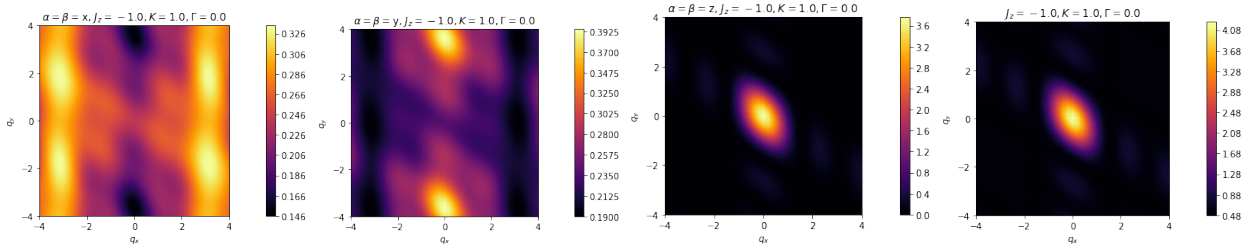

(a) xx (b) yy (c) zz (d) Ferromagnetic

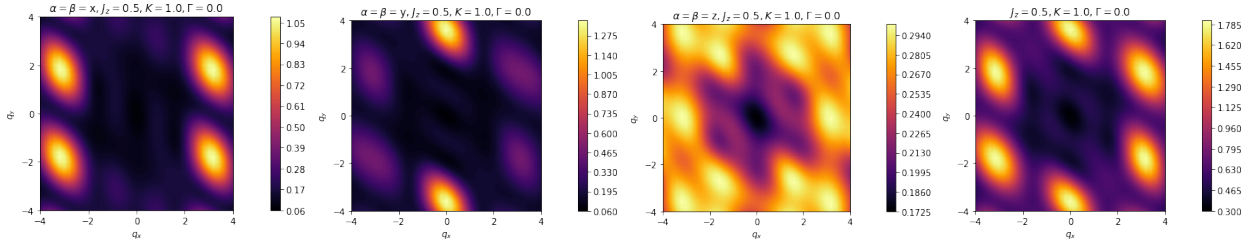

(e) xx (f) yy (g) zz (h) 2×2 in-plane

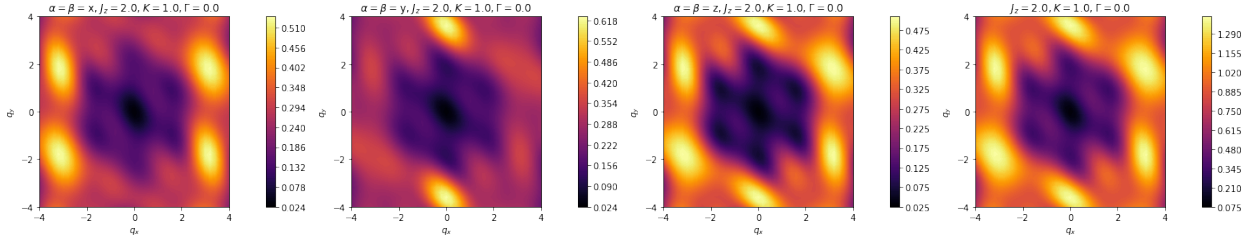

(i) xx (j) yy (k) zz (l) No order

Figure 5: Static spin structure factors for $\Gamma = 0$.

$J_z < -0.3$	$-0.3 < J_z < 1.2$	$J_z > 1.2$
Two-fold degeneracy Ferromagnetic	GS energy close to first few excited states 2×2 in-plane ordering	Nondegenerate, looks gapless Absence of order, plausible QSL phase

Table 1: Summary of results for $\Gamma = 0$

and large J_z.

Future work includes investigating whether rotational symmetry is broken—the static spin structure factor plots are not rotationally symmetric, counter to what we would expect at first glance. We should also determine whether the potential QSL phase is long-range entangled. We can compare our results to the magnetic orders obtained by the Luttinger-Tisza method. The Luttinger-Tisza method can be used to find ordered ground states in a classical spin model—the large spin limit of the quantum spin model. A large degeneracy in the ordered states' manifold suggests strong fluctuations and possible QSLs, so the Luttinger-Tisza method is a different approach analyze potential QSL models. Ultimately, this study provides a better understanding of whether the compound $Na_2BaCo(PO_4)_2$ hosts a QSL phase.

5 Acknowledgements

I would like to thank Dr. Yuan-Ming Lu for his mentorship, as well as Yonas Getachew and Wayne Zheng for their assistance. This REU program was primarily supported by the Center for Emergent Materials, part of an NSF Materials Research Science and Engineering Center (MRSEC), under award number DMR-1420451.

References

[1] Lucile Savary and Leon Balents. "Quantum spin liquids: a review". In: *Reports on Progress in Physics* 80.1 (Nov. 2016), p. 016502. ISSN: 1361-6633. DOI: 10.1088/0034-4885/80/1/016502. URL: http://dx.doi.org/10.1088/0034-4885/80/1/016502.

[2] Ruidan Zhong et al. "Strong quantum fluctuations in a quantum spin liquid candidate with a Co-based triangular lattice". In: *Proceedings of the National Academy of Sciences* 116.29 (2019), pp. 14505–14510. ISSN: 0027-8424. DOI: 10.1073/pnas.1906483116. eprint: https://www.pnas.org/content/116/29/14505.full.pdf. URL: https://www.pnas.org/content/116/29/14505.